Optics and Lasers in Engineering 183 (2024) 108496

Contents lists available at ScienceDirect

Optics and Lasers in Engineering

journal homepage: www.elsevier.com/locate/optlaseng

Review

Calibration method based on virtual phase-to-coordinate mapping with linear correction function for structured light system

Raul Vargas [a,*], Lenny A. Romero [b], Song Zhang [c], Andres G. Marrugo [a]

[a] Facultad de Ingeniería, Universidad Tecnológica de Bolívar, Cartagena, 130001, Bolivar, Colombia
[b] Facultad de Ciencias Básicas, Universidad Tecnológica de Bolívar, Cartagena, 130001, Bolivar, Colombia
[c] School of Mechanical Engineering, Purdue University, West Lafayette, 47907, IN, USA

ARTICLE INFO

Keywords:
Calibration
Structured light
Fringe projection
3D imaging

ABSTRACT

Structured light systems are crucial in fields requiring precise measurements, such as industrial manufacturing, due to their capability for real-time reconstructions. Existing calibration models, primarily based on stereo vision (SV) and pixel-wise approaches, face limitations in accuracy, complexity, and flexibility. These challenges stem from the inability to fully compensate for lens distortions and the errors introduced by physical calibration targets. Our work introduces a novel calibration approach using a virtual phase-to-coordinate mapping with a linear correction function, aiming to enhance accuracy and reduce complexity. This method involves traditional stereo calibration, phase processing, correction with ideal planes, and fitting a pixel-wise linear correction function. By employing virtual samples for phase-coordinate pairs and computing a pixel-wise correction, our methodology overcomes physical and numerical limitations associated with existing models. The results demonstrate superior measurement precision, robustness, and consistency, surpassing conventional stereo and polynomial regression models, both within and beyond the calibrated volume. This approach offers a significant advancement in structured light system calibration, providing a practical solution to existing challenges.

1. Introduction

Structured light systems are increasingly used across diverse fields, such as industrial manufacturing [1,2], medicine and bioscience [3,4], communications [5], and forensic sciences [6], because of their ability to address the metrological requirements of applications that require precise measurements across different scales [7] and real-time or high-speed reconstructions of dynamic objects or scenes [8]. The most widely employed calibration methodologies are based on stereo vision (SV) and pixel-wise models. However, these calibration methodologies still face challenges and limitations in guaranteeing the demands of different application fields, which may require low mathematical complexity models, low information processing times, and high flexibility in calibration procedures, among other requirements [9].

SV calibration models use the pinhole model with lens distortion and treat the projector as a reverse camera, representing the camera-projector system as a binocular stereo system [10]. This calibration approach has been largely successful, and is the most widely employed approach [7]. However, this model still has challenges in fully compensating for residual errors associated with lens distortions [11]. Moreover, these residual errors are often difficult to model properly and have been linked to the limitations of the physical target [12].

Alternatively, pixel-wise models based on nonlinear functions have been shown to effectively adapt to the camera-projector system nonlinearities [13]. However, fitting these models often requires sampling techniques in 3D space by precisely displacing manufactured pattern objects using translation stages to reliably relate the captured phase with the 3D coordinates [14]. It follows that regressions performed with the sampled 3D data may still contain errors owing to misalignment, positioning, and fabrication inaccuracies of the calibration objects and systems [15].

To improve the performance of calibration models, different strategies have been proposed to address the different error sources. For example, several studies have focused on compensating for errors caused by projector distortions by using pre-deformed fringe patterns or color fringe projections [16–19]. However, these strategies require additional calibration procedures or parameter optimization algorithms, thereby increasing the complexity of the calibration process.

Other proposed strategies are based on hybrid calibration procedures in which the stereo model is used as a positioning system to perform

* Corresponding author.
E-mail address: ravargas@utb.edu.co (R. Vargas).

https://doi.org/10.1016/j.optlaseng.2024.108496
Received 8 April 2024; Received in revised form 18 July 2024; Accepted 4 August 2024
Available online 16 August 2024

phase-coordinate pixel-wise mapping. Vargas et al. [13] proposed a hybrid calibration procedure in which stereo calibration was performed followed by the reconstruction of a manually displaced white plane across a depth range. However, this methodology requires an additional calibration procedure compared with the traditional stereo method, which increases the complexity and implementation time. Besides, other works as in Ref. [20] and Ref. [21] suggest using the extrinsic positions or 3D reconstruction of the stereo calibration targets to establish a pixel-wise polynomial regression model applied to unidirectional structured light systems. These approaches successfully compensate for residual errors in the stereo model without requiring additional procedures. However, employing the same stereo calibration targets makes it impossible to achieve proper and homogeneous sampling of the analyzed 3D space, which may lead to numerical errors when fitting the phase-coordinate regression models. Moreover, using polynomial functions can also introduce fitting issues such as the Runge phenomenon when a high polynomial order is employed and errors in extrapolating coordinates beyond the calibrated volume [15].

In this article, we propose a new approach to compensate for residual errors in the stereo calibration model through a pixel-wise linear correction function. This function is established by linking the experimental data from the stereo calibration procedure to virtual samples of phase-coordinate pairs, and computing a pixel-wise correction rigid transformation. The linear correction function thus circumvents the physical limitations and potentially numerical ill-conditions inherent to experimental sampling. The proposed methodology consists of four steps: 1) projection and capture of information for traditional stereo calibration, 2) phase processing and obtaining stereo parameters, 3) correction of experimental points with ideal planes and fitting of the pixel-wise linear correction function, and 4) virtual phase-to-coordinate mapping with linear error correction. The results demonstrate that our proposed methodology exhibits high measurement precision, robustness, and consistency, both within and beyond the experimentally sampled calibration volume, compared with the traditional stereo model and the polynomial regression models fitted from experimental calibration data.

2. Principle

2.1. Stereo vision model

A structured light (SL) system can be considered a binocular setup where both the camera and the projector can be mathematically modeled with the linear pinhole lens model as [10]

$$s^c[u^c, v^c, 1]^T = \mathbf{K^c}[\mathbf{I},\ \mathbf{0}][x, y, z, 1]^T \ , \tag{1}$$

$$s^p[u^p, v^p, 1]^T = \mathbf{K^p}[\mathbf{R}(\theta_s),\ \mathbf{t_s}][x, y, z, 1]^T \ , \tag{2}$$

where $[x, y, z]^T$ is a 3D point respecting the camera coordinate system, $[u^c, v^c]$ and $[u^p, v^p]$ are the projection of the point in the image plane of the camera and projector, respectively; $\mathbf{K}^c$ and $\mathbf{K}^p$ are the 3×3 intrinsic parameter matrices of camera and projector, $\mathbf{I}$ is a 3×3 identity matrix, $\mathbf{0}$ is a 3×1 zero vector, $\mathbf{R}(\theta_s)$ is a 3×3 rotation matrix and θ_s denotes a 3×1 vector with the Euler angles; $\mathbf{t}_s$ is a 3×1 translation vector; and s^c and s^p are scaling factors.

This projection model must be complemented with a lens distortion model to compensate for non-linearities of the optical system. This model can be established for both the camera and the projector as,

$$\begin{bmatrix}\bar{u}_d\\ \bar{v}_d\end{bmatrix} = (1 + k_1r^2 + k_2r^4 + k_3r^6)\begin{bmatrix}\bar{u}\\ \bar{v}\end{bmatrix} + \begin{bmatrix}2\rho_1\bar{u}\bar{v} + \rho_2(r^2 + 2\bar{u}^2)\\ 2\rho_2\bar{u}\bar{v} + \rho_1(r^2 + 2\bar{v}^2)\end{bmatrix}, \tag{3}$$

where $r^2 = \bar{u}^2 + \bar{v}^2$, $[k_1,\ k_2,\ k_3]$ are the radial distortion coefficients and $[\rho_1, \rho_2]$ are the tangential distortion parameters. $[\bar{u}_d, \bar{v}_d]^T$ refer to the distorted normalized points, and $[\bar{u}, \bar{v}]^T$ are the normalized coordinates without distortion given by

$$[\bar{u}, \bar{v}, 1]^T = \mathbf{K}^{-1}[u, v, 1]^T, \tag{4}$$

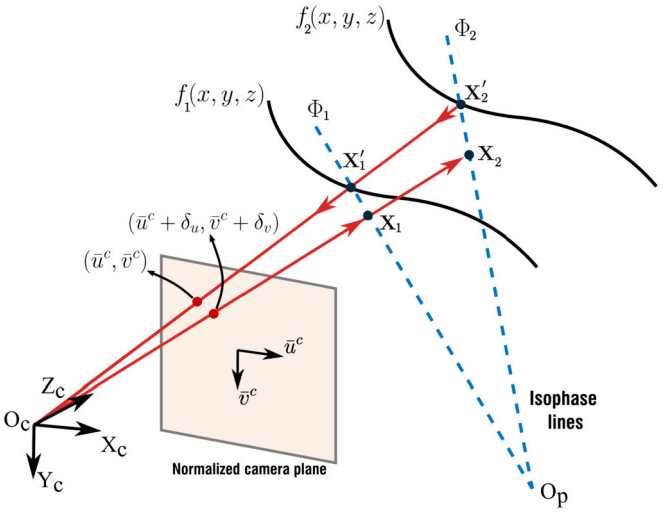

Fig. 1. Residual errors problem of 3D reconstruction of the stereo model.

where $\mathbf{K}^{-1}$ represents the inverse intrinsic parameter matrix. In this way, the distortion parameters for the camera and the projector can be denoted as $\mathbf{Dis}^c = [k_1^c,\ k_2^c,\ k_3^c,\ \rho_1^c,\ \rho_2^c]$ and $\mathbf{Dis}^p = [k_1^p,\ k_2^p,\ k_3^p,\ \rho_1^p,\ \rho_2^p]$, respectively.

The reconstruction process by means of this stereo model consists of obtaining the solution of the Equations (1), (2) and (4) for the coordinates $[x, y, z]^T$ as,

$$z = -\frac{m_{14} - m_{34}\bar{u}^p}{(m_{11} - m_{31}\bar{u}^p)\bar{u}^c + (m_{12} - m_{32}\bar{u}^p)\bar{v}^c + m_{13} - m_{33}\bar{u}^p} \tag{5}$$

$$x = \bar{u}^c z, \tag{6}$$

$$y = \bar{v}^c z, \tag{7}$$

where m_{ij} refers to the values of the i-th row and j-th column in a 3x4 matrix $M = [\mathbf{R}(\theta_s),\ \mathbf{t}_s]$.

2.2. Pixel-wise linear correction function

According to Equations (5)-(7), the reconstructed coordinates x, y, and z coordinates are dependent on the distortion-free normalized coordinate values $(\bar{u}^c, \bar{v}^c)$, which are calculated using the stereo parameters of the system. Thus, if our model has residual errors in estimating these calibration parameters, it can result in inaccuracies in the reconstruction process. In Fig. 1, we show the associated problem, in which a point $\mathbf{X}_1' = [x', y', z']$ that belongs to a surface $f_1(x, y, z)$ is illuminated by an isophase ray from the projector. This point is projected towards the camera, intercepting the normalized plane at a corresponding point $(\bar{u}^c, \bar{v}^c)$, which we can relate to a point captured in the pixel image plane as (u_d^c, v_d^c). During the 3D reconstruction process, the pixel (u_d^c, v_d^c) is projected onto the normalized plane using the calibration parameters obtained at a coordinate $(\bar{u}^c + \delta_u, \bar{v}^c + \delta_v)$, where (δ_u, δ_v) are residual errors of the stereo model due the estimation error of the parameters. As a result, when we triangulate this point with the same isophase ray, the 3D coordinate is estimated at the coordinate $\mathbf{X}_1 = [x, y, z]$. Besides, if the object is at a greater depth, the reconstruction errors will be larger.

If we consider that both points are referenced from the same coordinate origin, we can establish a vector relationship between points X and X' as,

$$[x', y', z']^T = \alpha\mathbf{R}[x, y, z]^T \tag{8}$$

where $\mathbf{R}$ is a rotation matrix, α is a scale factor and $(.)^T$ denotes the transpose operation. This equation can be rewritten as,

$$[x', y', z']^T = \begin{bmatrix} (\alpha R_{11})x + (\alpha R_{12}y + \alpha R_{13}z) \\ (\alpha R_{22})y + (\alpha R_{21}x + \alpha R_{23}z) \\ (\alpha R_{33})z + (\alpha R_{31}x + \alpha R_{32}y) \end{bmatrix}, \tag{9}$$

where R_{ij} are the coefficients of the matrix $\mathbf{R}$ corresponding to the i-th row and the j-th column. Furthermore, if we guarantee the independence and orthogonality between the corresponding axes of the coordinate (x, y, z), we can establish an approximation of the expression as,

$$\begin{bmatrix} x' \\ y' \\ z' \end{bmatrix} = \begin{bmatrix} \alpha_x x + \beta_x, \\ \alpha_y y + \beta_y, \\ \alpha_z z + \beta_z, \end{bmatrix} \tag{10}$$

where $[\alpha_x, \beta_x]$, $[\alpha_y, \beta_y]$ and $[\alpha_z, \beta_z]$ are the parameters of the linear relationship between $x' - x$, $y' - y$ and $z' - z$, respectively.

2.3. Phase-to-coordinate mapping

The phase-to-coordinate mapping (PCM) model aims to establish a direct and independent relationship between the camera-projector system and the metric coordinates (x, y, z) and the captured phase values for each pixel of the image (i, j). Among the mathematical models commonly used, the pixel-wise polynomial models are widely adopted and are defined as

$$x_{(i,j)} = \sum_{n=1}^{N} a_{n(i,j)} \phi^n_{(i,j)} \ , \tag{11}$$

$$y_{(i,j)} = \sum_{n=1}^{N} b_{n(i,j)} \phi^n_{(i,j)} \ , \tag{12}$$

$$z_{(i,j)} = \sum_{n=1}^{N} c_{n(i,j)} \phi^n_{(i,j)} \ , \tag{13}$$

where N is the degree of the polynomial, a_n, b_n, and c_n are the coefficients of the polynomials that relate the coordinates x, y, z with the phase values for each camera pixel. To obtain the coefficients of the polynomial, it is necessary to precisely and reliably position a target of known dimensions within a range of depth, in order to define the x, y, z coordinates with great accuracy. These coordinates are then related to the recovered phase from the projected fringe patterns, and the polynomial coefficients can be obtained through a least squares method.

The phase can be obtained by using phase-shifting fringe patterns [8]. For the N-step phase-shifted patterns, the wrapped phase φ is given by

$$\varphi = -\tan^{-1}\left[\frac{I_k \sin(2k\pi/N)}{I_k \cos(2k\pi/N)}\right] \ , \tag{14}$$

where I_k is the $k - th$ fringe pattern.

The arctangent function yields a discontinuous 2π-modulus phase map. Phase unwrapping is required to produce a smooth phase map prior to 3D reconstruction [22]. It is carried out by adding an integer number κ of 2π to each point accordingly, as

$$\phi = \varphi + 2\pi \times \kappa \ , \tag{15}$$

where ϕ is the unwrapped phase, and κ is the fringe order.

If we use a conventional black and white calibration target, the recovered phase may have phase artifacts due to the black to white transitions in edges. To overcome, this problem Vargas et al., [13] and Zhang [20] used phase a phase smoothing approach using 2D polynomials as,

$$\Phi(u, v) = \sum_{n=0}^{N} \sum_{m=0}^{M} a_{nm} u^m v^n, \tag{16}$$

where N and M are the degrees of the 2D polynomial for the u and v coordinates, respectively. u and v are the pixel coordinates, a_{nm} are the polynomial coefficients, and Φ is the phase adjusted as a function of u and v for the calibration target. The presence of error can also be compensated with other interpolation or filtering strategies, or by using special targets or color fringes [23].

2.4. Virtual phase-to-coordinate mapping

In this article, we present a virtual PCM method utilizing the stereo parameters obtained from an experimentally calibrated camera-projector system. The proposed calibration procedure involves the consideration of an infinite virtual plane positioned at various distances z_n from the camera and perpendicular to it. This virtual plane is displaced in N positions from a distance z_0 to z_{N-1}. The process requires establishing the metric coordinates for each pixel (i, j) on the n-th plane captured by the camera, as well as its corresponding phase value. We can establish a relationship between the camera image coordinate system and the virtual planes by means of Equation (1) as,

$$\alpha^c \begin{bmatrix} u^c \\ v^c \\ 1 \end{bmatrix} = K^c \begin{bmatrix} 1 & 0 & 0 & 0 \\ 0 & 1 & 0 & 0 \\ 0 & 0 & 1 & 0 \end{bmatrix} \begin{bmatrix} \hat{x} \\ \hat{y} \\ \hat{z} \\ 1 \end{bmatrix}, \tag{17}$$

with

$$K^c = \begin{bmatrix} f^c_u & 0 & c^c_u \\ 0 & f^c_v & c^c_v \\ 0 & 0 & 1 \end{bmatrix}, \tag{18}$$

where $[f^c_u, f^c_v]$ is the focal length of the camera in pixels, $[u^c_c, v^c_c]$ is the coordinate of the principal point, and $[\hat{x}, \hat{y}, \hat{z}]$ represent the virtual coordinate that is projected onto a point $[u^c, v^c]$ in the camera image plane, which is obtained by applying a correction of a integer pixel coordinates (i, j), using the distortion parameters $\mathbf{Dist}^c$. Thus, for each pixel (i, j) and each virtual plane n, we can establish the virtual coordinates $[\hat{x}, \hat{y}, \hat{z}]$ as,

$$\hat{x}_{n(i,j)} = \frac{z_n}{f^c_u}(u^c_{(i,j)} - c^c_u), \tag{19}$$

$$\hat{y}_{n(i,j)} = \frac{z_n}{f^c_v}(v^c_{(i,j)} - c^c_v), \tag{20}$$

$$\hat{z}_{n(i,j)} = z_n. \tag{21}$$

To calculate the phase value, we project the virtual point onto the projector image plane using Equation (2) to obtain the coordinates (u^p, v^p). Then, we apply the distortion parameters $\mathbf{Dist}^p$ to these coordinates to calculate the distorted coordinate (u^p_d, v^p_d), which can be converted to phase as,

$$\hat{\phi}_{u(i,j)} = u^p_{d(i,j)} \cdot \frac{2\pi}{P}, \tag{22}$$

$$\hat{\phi}_{v(i,j)} = v^p_{d(i,j)} \cdot \frac{2\pi}{P}, \tag{23}$$

where the P is the pitch (i.e., number of pixels per fringe) of the projected phase-shifted fringe patterns.

3. Proposed method

In this article, we propose a calibration methodology that consists of virtual data correction based on experimental data obtained from the stereo calibration process. This approach does not require additional experimental procedures beyond the conventional stereo calibration method. The proposed methodology is based on the following four steps:

Step 1: projection and capture

In this initial stage, the fringe patterns are projected onto a calibration target and captured at different positions and orientations spanning a range of depths.

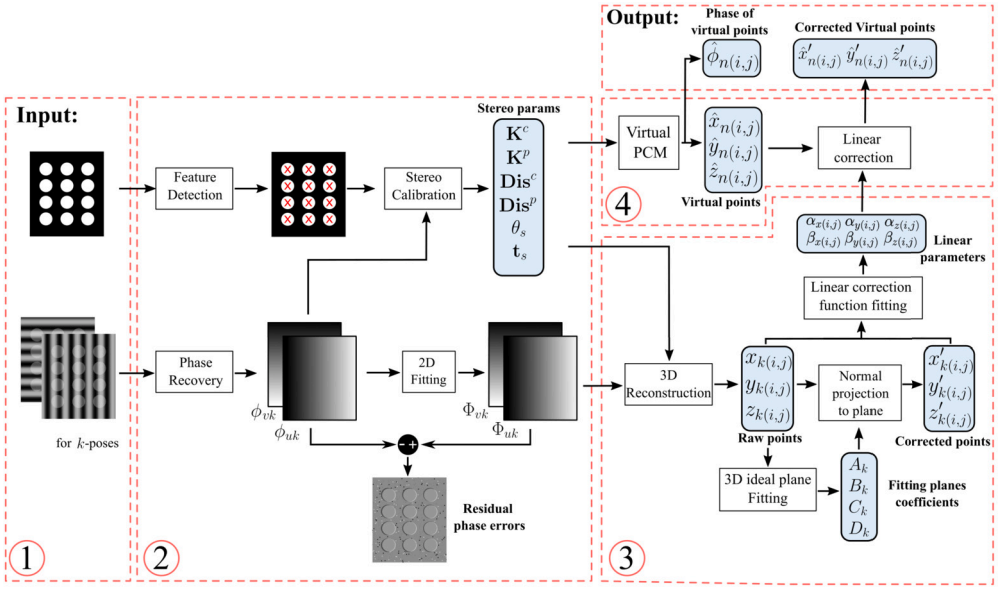

Fig. 2. Framework of the proposed four-steps methodology: (1) Projection and capture, (2) Phase and stereo calibration, (3) Adjustment of the correction function using ideal planes, and (4) Virtual PCM with linear correction of coordinates.

Step 2. phase and stereo calibration

In this step, we detect the centers of circles on the calibration target for each position and orientation k, and extract the continuous phase from the projected fringe patterns. Since the circle centers in the images are detected with subpixel precision and the phase maps are obtained at the pixel level, an interpolation procedure is necessary to determine the phase value for each circle center on the target. In this bilinear interpolation process, we use the four neighboring pixels around the detected center and their respective phase values. These phase values are then converted to projector pixel coordinates using the fringe step of the projected pattern. Finally, the correspondences between the circles on the target from the camera and the projector are used to calculate the stereo parameters of the system using a camera calibration toolbox. Simultaneously, we perform a 5th-order 2D polynomial fit of the phase maps to eliminate any errors caused by circle borders and noise in the black background of the target, obtaining an adjusted phase surface described in Equation (16).

Step 3. adjustment of the correction function using ideal planes

In this step, we use the stereo parameters and the adjusted phase Φ_k obtained in the previous step to calculate the 3D coordinate $[x_{k(i,j)}, y_{k(i,j)}, z_{k(i,j)}]$ corresponding to each integer camera pixel (i,j) for each k-pose. Subsequently, each k reconstruction is fitted to an ideal plane as,

$$A_k x_{k(i,j)} + B_k y_{k(i,j)} + C_k z_{k(i,j)} + D_k = 0, \tag{24}$$

where A_k, B_k, C_k, and D_k are the coefficients of the fitted plane, which can be calculated using least squares. Due to the presence of residual errors in the stereo model explained in Section 2.2, the reconstructed points are deviated from the ideal plane. To obtain the corrected coordinates of each point on the plane, we propose projecting the point onto the plane in the normal direction as,

$$\begin{bmatrix} x'_{k(i,j)} \\ y'_{k(i,j)} \\ z'_{k(i,j)} \end{bmatrix} = \begin{bmatrix} x_{k(i,j)} \\ y_{k(i,j)} \\ z_{k(i,j)} \end{bmatrix} - \delta_{k(i,j)} \frac{\vec{\mathbf{n}}_k}{||\vec{\mathbf{n}}_k||}, \tag{25}$$

where $[x'_{k(i,j)}, y'_{k(i,j)}, z'_{k(i,j)}]^T$ is the corrected coordinate, $\delta_{k(i,j)}$ is the perpendicular distance between the plane and each point, and $\vec{\mathbf{n}}_k = [A_k, B_k, C_k]^T$ represents the vector normal to the k-plane, and $||.||$ represents the length of the vector. Finally, we relate the reconstructed and corrected coordinates for each pixel as an independent linear function of the plane position k, by calculating the parameters $\alpha_x, \beta_x, \alpha_y, \beta_y, \alpha_z$ and β_z defined in equation (10), using the least squares method.

Step 4. virtual PCM with linear correction of coordinates

Using the stereo parameters obtained in Step 2, we carry out a Virtual PCM as described in Section 2.4. The simulation is performed by displacing a virtual plane in n-positions through a given depth range and calculating the coordinates $(\hat{x}_{n(i,j)}, \hat{y}_{n(i,j)}, \hat{z}_{n(i,j)})$ for each pixel projected onto the virtual plane and its corresponding phase value $\hat{\phi}_{n(i,j)}$. Then, using the parameters of the linear correction model obtained in Step 3, the virtual points can be corrected by,

$$\begin{bmatrix} \hat{x}'_{n(i,j)} \\ \hat{y}'_{n(i,j)} \\ \hat{z}'_{n(i,j)} \end{bmatrix} = \begin{bmatrix} \alpha_{x(i,j)} \hat{x}_{n(i,j)} + \beta_{x(i,j)} \\ \alpha_{y(i,j)} \hat{y}_{n(i,j)} + \beta_{x(i,j)} \\ \alpha_{z(i,j)} \hat{z}_{n(i,j)} + \beta_{x(i,j)} \end{bmatrix}. \tag{26}$$

As shown in Fig. 2, the output of the calibration procedure are the corrected virtual coordinates $\hat{x}'_{n(i,j)}$, $\hat{y}'_{n(i,j)}$, $\hat{z}'_{n(i,j)}$ and their corresponding phase values $\hat{\phi}_{n(i,j)}$. This information is then used to set the phase-to-coordinates mapping functions for each pixel (i,j) as

$$\hat{x}' = f_1(\hat{\phi}), \tag{27}$$

$$\hat{y}' = f_2(\hat{\phi}), \tag{28}$$

$$\hat{z}' = f_3(\hat{\phi}), \tag{29}$$

where f_1, f_2, and f_3 are functions that relate the phase values and the 3D coordinates. Thus, any type of regression function or a look-up table (LUT) can be corrected using the linear error correction method. In this work, we perform the correction of polynomial functions since they are one of the most commonly used and also present significant numerical fitting challenges. To perform the 3D reconstruction process, these functions are used to evaluate the captured phase, resulting in the reconstructed coordinates.

Fig. 2 shows a graphical summary of the proposed four-step methodology, illustrating the inputs and outputs of each procedure.

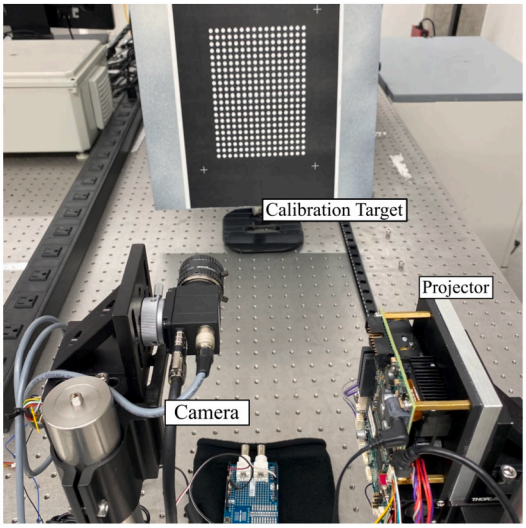

Fig. 3. System setup.

4. Experimental results

System setup

We evaluated the proposed calibration methodology using the experimental system shown in Fig. 3, which is composed of a CMOS camera (FLIR Blackfly BFS-U3-28S5M-C) and a DLP projector (LightCrafter 4500). The camera was attached with a 16 mm focal length lens (Computar M1614-MP2) and adjusted to a resolution of 1600×1200 pixels, while the projector was configured with a native resolution of 960×1440. For the calibration and reconstruction procedures, we projected binary patterns of vertical and horizontal fringe patterns with a period of 18 pixels. We applied an 18-step phase-shifting algorithm and a 6-bit Gray binary coding algorithm to recover the absolute continuous phase maps of the captured patterns. For our system configuration, the highest sensitivity was obtained with the phase map obtained from horizontal fringes, i.e., ϕ_v. Therefore, we used this phase map to relate the 3D coordinates.

Calibration system and linear correction function fitting

The system was calibrated using a conventional stereo technique using a 16×21 circle pattern at 25 positions, which are reported in the Table 1. Using these parameters and the adjusted maps of the targets, we reconstructed the target in its 25 positions. Then, following our proposed correction methodology, we performed an adjustment to an ideal plane using least squares and corrected pixel by projecting them onto the ideal plane. Fig. 4(a) shows the error map of the adjustment to an ideal plane at the Position 12 of the target, and Fig. 4(b) shows the 3D visualization of the error, with the adjusted plane as reference. We can observe that the obtained reconstruction is not completely flat and presents greater errors near the edges of the image, where there is presumed to be a greater presence of distortions and even areas that are not adequately sampled by the target's control points. Fig. 4(c)-(e) show the reconstructed coordinates (x_k, y_k, z_k) for the 25 reconstructed positions of the target at pixel $(960, 1280)$ and the corrected coordinates upon projection onto the ideal plane (x'_k, y'_k, z'_k). These coordinates are related to the same associated phase value, which corresponds to the phase value captured by pixel $(960, 1280)$ at each position k of the target. Fig. 4(f)-(h) show the relationship between the reconstructed and corrected coordinates for pixel index (960, 1280), and we compute the linear relationship between these coordinates using the Equation (26).

Virtual sampling and linear correction

Table 1
System parameters obtained with the stereo calibration method. Mean reprojection errors in pixels: projector (0.1407), camera (0.2528), and stereo (0.1967).

Stereo parameters
$\boldsymbol{K}^c = \begin{bmatrix} 3594.8 & 0 & 795.1 \\ 0 & 3594.5 & 626.0 \\ 0 & 0 & 1 \end{bmatrix}$
$\boldsymbol{K}^p = \begin{bmatrix} 1120.4 & 0 & 459.9 \\ 0 & 2248.9 & 1149.3 \\ 0 & 0 & 1 \end{bmatrix}$
$\mathbf{Dist}^c$ = [-0.1124 0.2740 0 0.0002 -0.0007]
$\mathbf{Dist}^p$ = [0.0932 -0.2802 0 0.0032 -0.0031]
θ_s [°] = [2.87 0.75 -179.72]
$\mathbf{t}_s$ [mm] = [21.9868 -137.5459 28.2896]

Once we have established our correction function for each pixel, we proceed to perform a virtual sampling of coordinates using the stereo parameters of our system. Fig. 5(a) shows a schematic of the virtual sampling procedure, in which n =30 equidistant virtual planes were positioned in a depth range of 350 mm to 950 mm from the camera. Then, for each pixel (i, j), we calculate the corresponding virtual coordinates $(\hat{x}_n, \hat{y}_n, \hat{z}_n)$ of each n-plane, and its phase value $\hat{\phi}_n$. Fig. 5(b) shows the $\hat{z}_n$ coordinate vs the corresponding phase obtained from this sampling for the pixel $(960, 1280)$, and the resulting $\hat{z}'_n$ coordinate after the proposed linear correction. We can see that the points are very similar, however, they present a slight difference after the error compensation.

Fig. 6(a) displays the resulting polynomials from a regression performed on the corrected experimental z-coordinate of the points (z'_k) and their corresponding captured phases for the pixel $(960, 1200)$. The polynomials fit the data adequately in the 500 mm-700 mm range, but become unstable outside this area, especially at higher orders. This instability stems from non-uniform experimental data sampling and the inherent susceptibility of polynomials to extrapolation or interpolation errors. Fig. 6(b) illustrates the outcome of polynomial regressions using the corrected virtual coordinates and their corresponding phase (our proposed method), which provide a broader depth and more evenly distributed data points. The polynomial models demonstrate enhanced numerical stability across a wider range. However, the third-order polynomial does not adequately fit the data in the central depth region corresponding to the experimental points, suggesting the need for higher order polynomials for a more accurate description of the entire depth range. Crucially, our proposed method enables the use of these higher-order polynomials without the usual issues associated with limited sampling.

5. Validation experiments

5.1. Flat board reconstruction

The first experiment aimed to reconstruct a plane, specifically the back of a mirror, in 20 different positions and orientations. Each position was reconstructed using The stereo model and the polynomial regression models POL3-E, POL6-E, POL3-V, and POL6-V. Where POL3-E and POL6-E refer to a third and sixth degree polynomial regression, respectively, using the experimental raw data of the calibration targets. POL3-V and POL6-V correspond to a polynomial regression of third and sixth degree, respectively, using the corrected virtual data based on our proposed methodology. Using these models, we calculated the RMS fitting error to an ideal plane for each reconstruction.

The RMS errors achieved for each plane pose for the calibration models are presented in Fig. 7. The results indicate that the error generated by the stereo model is consistent and uniform across all analyzed reconstructed positions of the plane. Conversely, models derived from direct regressions with experimental data (POL3-E and POL6-E) exhibit reconstruction errors lower than those of the stereo model in the initial poses

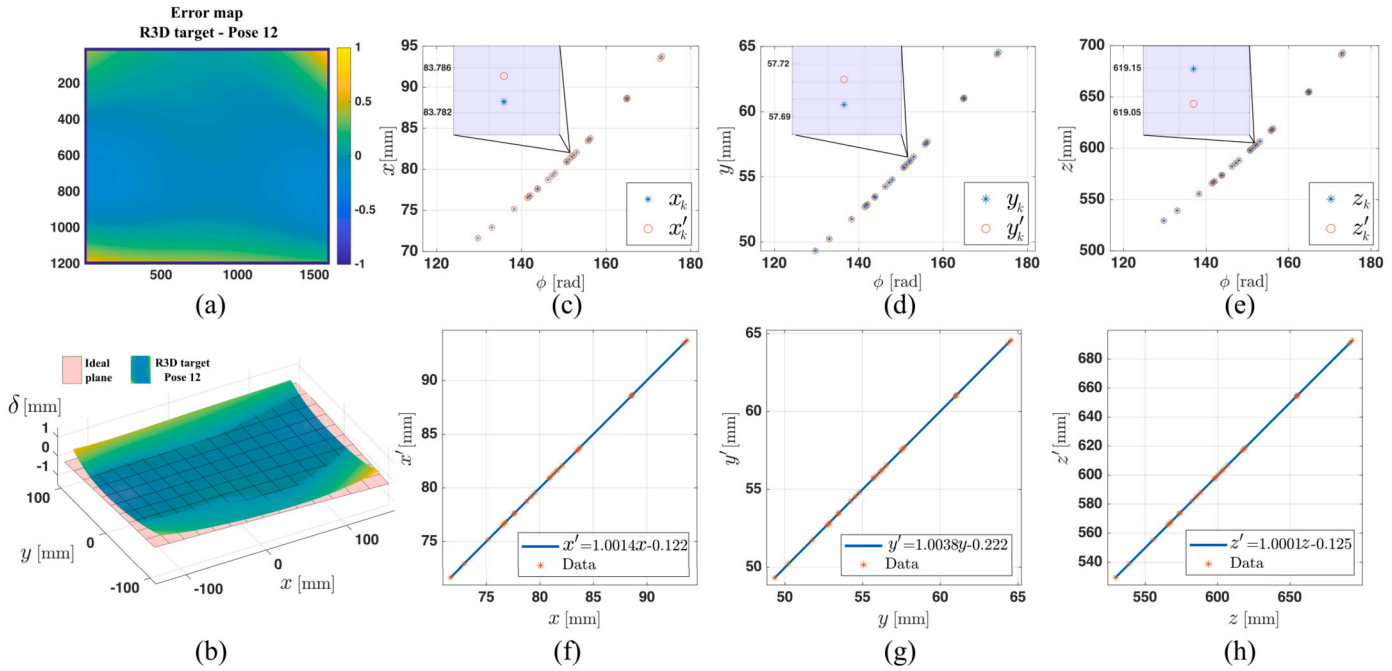

Fig. 4. Linear correction function fitting. (a) Fit error map to an ideal plane of the reconstructed calibration target at position 12 using the stereo model. (b) 3D visualization of the error map. (c)-(e) reconstructed (x, y, z) and corrected (x', y', z') coordinates for the 25 positions of the calibration target versus their respective phase values captured for pixel $(960, 1280)$. (f) -(h) Linear adjustment between the reconstructed coordinates and the corrected coordinates.

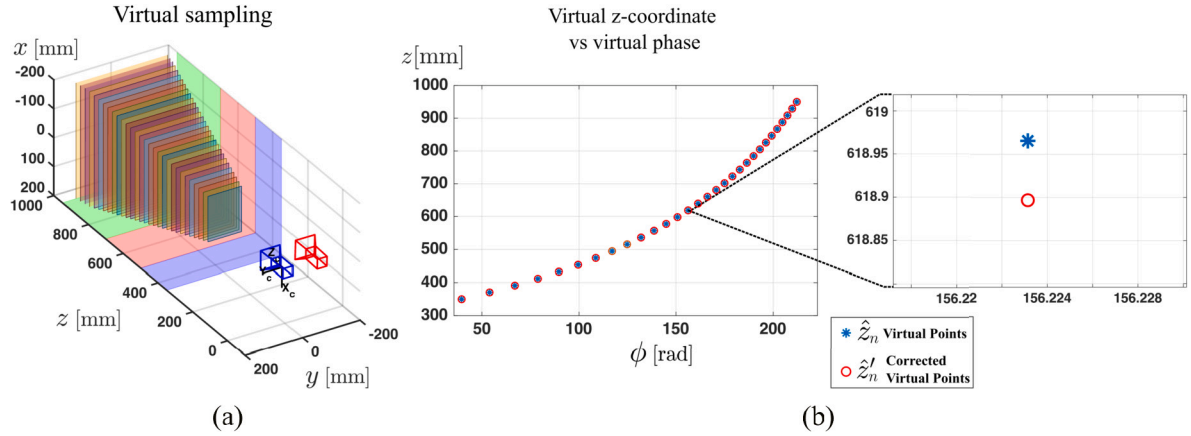

Fig. 5. (a) Virtual mapping scheme. (b) $\hat{z} - \phi$ is the relationship between depth and phase for a pixel (960,1200) using the proposed virtual mapping, and $\hat{z}' - \phi$ is the corrected relationship after applying the linear correction function proposed.

of the plane, corresponding to poses within the experimental calibration volume. However, beyond the ninth pose, these models demonstrate high reconstruction errors, particularly for the sixth-order polynomial (POL6-E), where errors escalate due to numerical instability of the polynomial for extrapolating information. Besides, polynomial models fitted with our proposed method, two distinct behaviors are observed. In the case of POL3-V, some positions exhibit lower errors compared to those obtained from traditional methods, while in others, errors increase significantly. In contrast, the POL6-V model yields much lower reconstruction errors across all positions of the planes compared to the stereo model and the other regression models. These findings demonstrate that our methodology enables greater system precision and compensates for errors associated with the stereo reconstruction model. Nevertheless, it remains crucial to adjust a function capable of accurately representing the phase-coordinate corrected relationship.

Fig. 8 shows the error maps, error histograms, and 3D pose of the plane for pose 17. We observe that the plane is both inside and outside the calibrated volume. For this position, the experimental regression models POL3-E and POL6-E exhibit a strong reconstruction error, with errors even exceeding 2 mm. Comparing the POL3-V, POL6-V and traditional stereo models, we can see that our proposed calibration methodology compensates for residual errors present in the traditional stereo model. The error histogram shows that our method allows for a better error distribution, with a mean close to zero and low dispersion. The analysis of the other poses can be seen in Visualization 1.

5.2. Sphere reconstruction

In the second experiment, we aimed to reconstruct a sphere with a diameter of 196 mm and placed it in seven different positions, varying its transversal location and distance from the camera. Each pose was reconstructed using the stereo model and the polynomial models, and the reconstructed sphere was fitted to an ideal sphere to estimate its center and radius. Fig. 9 shows the error maps of the fittings, the error histogram, and the 3D positioning for the first pose of the sphere.

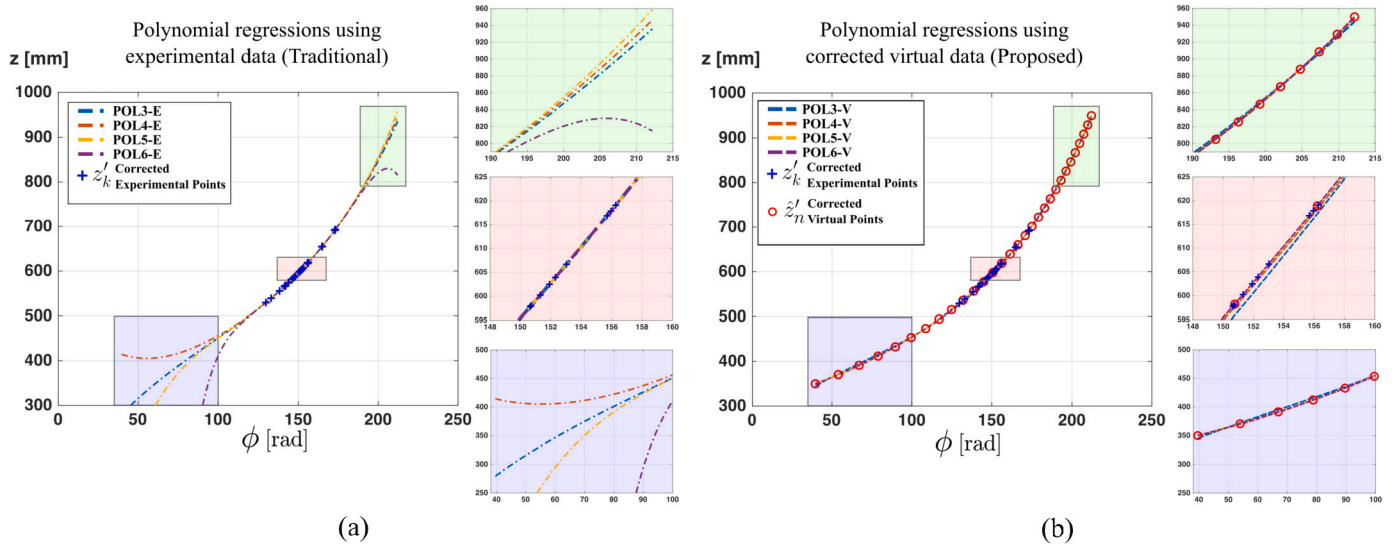

Fig. 6. Polynomial adjustment of different orders, for the pixel (960, 1200), using (a) the corrected experimental z'_k coordinates and the experimental phase; (b) the corrected virtual $\hat{z}'_n$ coordinates and the corresponding phase. The nomenclature POLX-E refers to a polynomial regression of degree X using experimental data of the calibration targets. While the nomenclature POLX-V corresponds to a polynomial regression of degree X obtained using the corrected virtual data based on our proposed methodology.

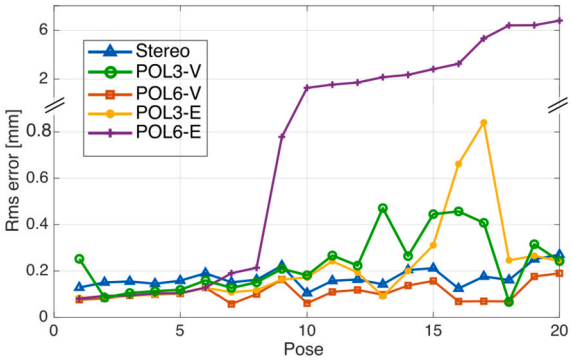

Fig. 7. RMS fitting error of a flat board (back of a mirror) in different positions and orientations reconstructed by the Stereo, POL6-V, POL3-E, and POL6-E models.

In this particular position, it is observable that the sphere was located beyond the depth sampled during calibration. Error maps reveal that the stereo model exhibits a uniform error across the field of view of the camera, whereas polynomial regression models POL3-E and POL6-E display transversal error variations. Conversely, regression models POL3-V and POL6-V generate highly uniform error maps with values close to zero. This demonstrates that direct polynomial regressions on experimental data can induce reconstruction errors across the captured transversal area, particularly when objects are positioned outside the calibrated volume. Our proposed calibration strategy mitigates such occurrences, thereby expanding the depth reconstruction range. Additionally, upon analyzing error histograms, we note that our proposed models yield reconstruction RMS errors of 0.080 mm and 0.072 mm, respectively, both below the RMS error of 0.109 mm obtained by the stereo model. The results for the other positions of the sphere can be seen in Visualization 2.

5.3. Complex shape reconstruction

Finally, we performed the reconstruction of a complex-shaped object to demonstrate that our proposed calibration methodology based on pixel-wise approach allows high-resolution and high-quality reconstructions while maintaining the shape and details of the objects. Fig. 10(a) shows the captured image of the object, and Fig. 10(b) shows the 3D model obtained, where we can observe that the proposed model does not alter the characteristics of the reconstructed objects, resulting in high-resolution reconstructions.

5.4. Analysis of error sources

The validation experiments show that the proposed methodology only functions adequately with a higher-degree polynomial; in this case, a sixth-order polynomial was used. This is because high-degree polynomials can fit the entire depth space sampled in the virtual mapping. The greater the mapped depth, the higher the order of the fitted polynomial must be. Consequently, we can observe the presence of residual errors in our proposed method when using a third-order polynomial in some reconstructions of the flat board and sphere, especially where the reconstructions extend beyond the calibrated volume. Despite this, our proposed methodology successfully avoids the ill-conditioning problems when fitting higher-degree polynomials to experimental data.

6. Conclusion

In this article, we proposed a new calibration strategy based on a pixel-wise error correction function and a virtual-theoretical model adjusted from experimental data. This methodology allowed us to obtain a uniform and extended mapping of the 3D measurement space, ensuring that the phase-coordinate models were robust to undersampling and numerical ill-conditioning issues. The experiments demonstrated that our methodology guaranteed high measurement accuracy both inside and outside the calibrated volume compared to the traditional stereo model and polynomial regression models commonly used.

The proposed methodology has great potential for utilization in high-precision 3D applications within large measurement fields because it eliminates the need for physical mapping of the 3D space. Furthermore, the pixel-wise error compensation methodology opens the door to new strategies for structured light system recalibration in which pixel-wise functions can be used to transform a base model and accurately describe the system with minimal captured experimental information. These advancements will allow for more efficient and flexible recalibration processes, thereby enhancing the adaptability of structured light systems in various applications.

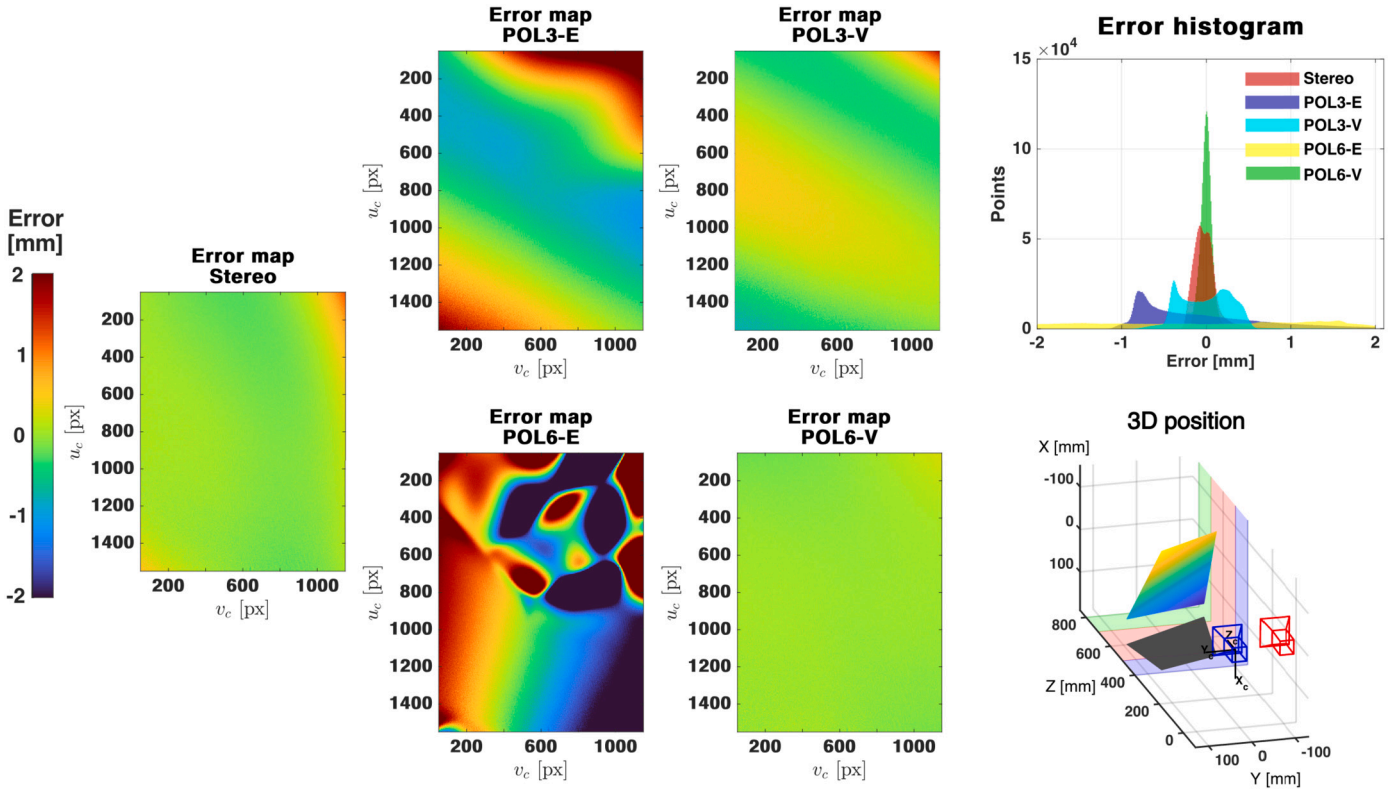

Fig. 8. Reconstruction of a flat board (back of a mirror) in pose 17 using the traditional Stereo model; polynomial regression models POL3-E and POL6-E, based on experimental data; and polynomial regression model POL3-V and POL6-V models, based on our proposed method. The error maps of the models show that our proposed method achieves a decrease in error along the observed transverse field. Furthermore, the error histogram shows us that the error distribution in our proposed method achieves a lower dispersion and a mean close to zero. To analyze the other poses, see Visualization 1.

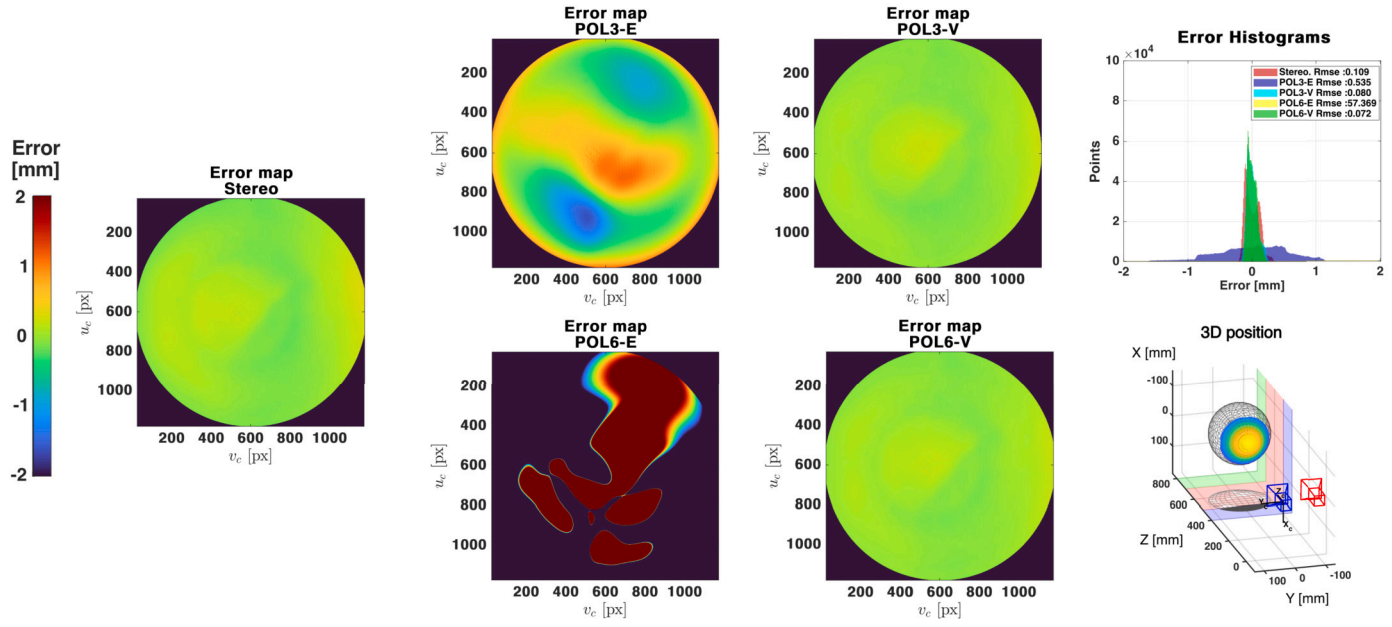

Fig. 9. Reconstruction results of a 192 mm diameter sphere in front of the calibration volume (Pose 1 of 7) using the Stereo, POL3-E, POL6-E, POL3-V, and POL6-V calibration models. The error maps are calculated by performing an adjustment to an ideal sphere of the reconstructions obtained for each model. This allows us to observe how the adjustment error varies throughout the image. The error histogram shows the distribution of the fitting error for the analyzed models. The 3D position shown corresponds to the reconstruction obtained from the POL6-V model. See the results of the other positions in Visualization 2.

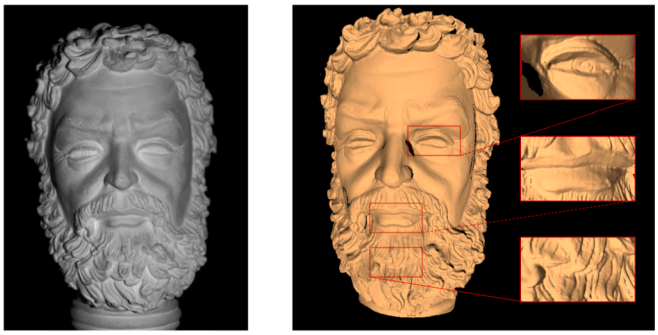

Fig. 10. Reconstruction of a complex shape using POL6-V model. (a) photography of the object. (b) High resolution 3D reconstruction.

CRediT authorship contribution statement

Raul Vargas: Writing – original draft, Validation, Software, Methodology, Investigation, Formal analysis, Data curation, Conceptualization. **Lenny A. Romero:** Writing – review & editing, Supervision, Project administration, Funding acquisition, Conceptualization. **Song Zhang:** Writing – review & editing, Supervision, Methodology. **Andres G. Marrugo:** Writing – review & editing, Writing – original draft, Supervision, Methodology, Investigation, Funding acquisition, Formal analysis, Conceptualization.

Declaration of competing interest

The authors declare the following financial interests/personal relationships which may be considered as potential competing interests: Raul Vargas reports financial support was provided by Tecnologica University of Bolivar. Song Zhang is an associated editor for OLEN. Song Zhang reports a relationship with Vision Express Optics Inc (Auburn Hills, Michigan, USA). that includes: board membership. Song Zhang reports a relationship with Orbbec3D Inc (Troy, Michigan, USA) that includes: consulting or advisory. Song Zhang reports a relationship with ORI LLC (Salt Lake City, Utah, USA). that includes: consulting or advisory. If there are other authors, they declare that they have no known competing financial interests or personal relationships that could have appeared to influence the work reported in this paper.

Data availability

Data will be made available on request.

Acknowledgement

When this research work was done, R. Vargas was a visiting scholar at Purdue University. R. Vargas thanks the Universidad Tecnológica de Bolívar (UTB) for a postgraduate scholarship and a Research Internship Fellowship.

Funding

Universidad Tecnológica de Bolívar (UTB) project CI2021P04.

Appendix A. Supplementary material

Supplementary material related to this article can be found online at https://doi.org/10.1016/j.optlaseng.2024.108496.

References

[1] Qian J, Feng S, Xu M, Tao T, Shang Y, Chen Q, et al. High-resolution real-time 360º 3d surface defect inspection with fringe projection profilometry. Opt Lasers Eng 2021;137:106382.
[2] Li B. High-speed 3d optical sensing for manufacturing research and industrial sensing applications. Trans Energy Syst Eng Appl 2022;3(2):1–12.
[3] Bacqueville D, Maret A, Noizet M, Duprat L, Coutanceau C, Georgescu V, et al. Efficacy of a dermocosmetic serum combining bakuchiol and vanilla tahitensis extract to prevent skin photoaging in vitro and to improve clinical outcomes for naturally aged skin. Clin Cosmet Invest Dermatol 2020:359–70.
[4] Pineda J, Vargas R, Romero LA, Marrugo J, Meneses J, Marrugo AG. Robust automated reading of the skin prick test via 3d imaging and parametric surface fitting. PLoS ONE 2019;14(10):e0223623.
[5] Bell T, Zhang S. Holo reality: real-time low-bandwidth 3d range video communications on consumer mobile devices with application to augmented reality. J Electron Imaging 2019;2019(16):7.
[6] Liao Y-H, Hyun J-S, Feller M, Bell T, Bortins I, Wolfe J, et al. Portable high-resolution automated 3d imaging for footwear and tire impression capture. J Forensic Sci 2021;66(1):112–28.
[7] Marrugo AG, Gao F, Zhang S. State-of-the-art active optical techniques for three-dimensional surface metrology: a review. JOSA A 2020;37(9):B60–77.
[8] Zhang S. High-speed 3D imaging with digital fringe projection techniques. CRC Press; 2018.
[9] Zhang S. Recent progresses on real-time 3d shape measurement using digital fringe projection techniques. Opt Lasers Eng 2010;48(2):149–58.
[10] Zhang S, Huang P. Novel method for structured light system calibration. Opt Eng 2006;45. https://doi.org/10.1117/1.2336196.
[11] Bu L, Wang R, Wang X, Hou Z, Zhou Y, Wang Y, et al. Calibration method for fringe projection profilometry based on rational function lens distortion model. Measurement 2023:112996.
[12] Liu Y, Zhang B, Yuan X, Lin J, Jiang K. An improved projector calibration method by phase mapping based on fringe projection profilometry. Sensors 2023;23(3):1142.
[13] Vargas R, Marrugo AG, Zhang S, Romero LA. Hybrid calibration procedure for fringe projection profilometry based on stereo vision and polynomial fitting. Appl Opt 2020;59(13):D163–9.
[14] Vargas R, Marrugo AG, Pineda J, Meneses J, Romero LA. Camera-projector calibration methods with compensation of geometric distortions in fringe projection profilometry: a comparative study. Opt Pura Appl 2018;51(3):1–10. https://doi.org/10.7149/OPA.51.3.50305.
[15] Feng S, Zuo C, Zhang L, Tao T, Hu Y, Yin W, et al. Calibration of fringe projection profilometry: a comparative review. Opt Lasers Eng 2021;143:106622.
[16] Juarez-Salazar R, Diaz-Ramirez VH. Flexible camera-projector calibration using superposed color checkerboards. Opt Lasers Eng 2019;120:59–65.
[17] Xing S, Guo H. Iterative calibration method for measurement system having lens distortions in fringe projection profilometry. Opt Express 2020;28(2):1177–96.
[18] Yu J, Gao N, Meng Z, Zhang Z. A three-dimensional measurement system calibration method based on red/blue orthogonal fringe projection. Opt Lasers Eng 2021;139:106506.
[19] Yu J, Gao N, Meng Z, Zhang Z. High-accuracy projector calibration method for fringe projection profilometry considering perspective transformation. Opt Express 2021;29(10):15053–66.
[20] Zhang S. Flexible and high-accuracy method for uni-directional structured light system calibration. Opt Lasers Eng 2021;143:106637.
[21] Marrugo AG, Vargas R, Romero LA, Zhang S. Method for large-scale structured-light system calibration. Opt Express 2021;29(11):17316–29.
[22] Zhang S. Absolute phase retrieval methods for digital fringe projection profilometry: a review. Opt Lasers Eng 2018;107:28–37.
[23] Zhang S. Pixel-wise structured light calibration method with a color calibration target. Opt Express 2022;30(20):35817–27.